Available online at www.sciencedirect.com
SCIENCE DIRECT
Journal of Solid State Chemistry 179 (2006) 1067–1075
JOURNAL OF SOLID STATE CHEMISTRY
www.elsevier.com/locate/jssc

Formation of crystalline $TiO_{2-x}N_x$ and its photocatalytic activity

Jum Suk Jang[a], Hyun Gyu Kim[b], Sang Min Ji[a], Sang Won Bae[a], Jong Hyeon Jung[c], Byung Hyun Shon[d], Jae Sung Lee[a,*]

[a]Department of Chemical Engineering, Institute of Environmental and Energy Technology, School of Environmental and Science Engineering, Pohang University of Science and Technology (POSTECH), San 31 Hyoja-dong, Pohang 790-784, Republic of Korea
[b]Busan Center, Korea Basic Science Institute (KBSI), Busan, 609-735, Republic of Korea
[c]Division of Biotechnology and Health Engineering, Sorabol College, Gyeongju 780-711, Republic of Korea
[d]Department of Environmental Engineering, Hanseo Unversity, Seosan 356-706, Republic of Korea

Received 28 April 2005; received in revised form 27 December 2005; accepted 1 January 2006
Available online 10 February 2006

Abstract

Amorphous precursors to nitrogen-doped TiO_2 (NTP) and pure TiO_2 (ATP) powders were synthesized by hydrolytic synthesis and sol–gel method (SGM), respectively. Corresponding crystalline phases were obtained by thermally induced transformation of these amorphous powders. From FT-IR and XPS data, it was concluded that a complex containing titanium and ammonia was formed in the precipitate stage while calcination drove weakly adsorbed ammonium species off the surface, decomposed ammonia bound on surface of precipitated powder and led to substitution of nitrogen atom into the lattice of TiO_2 during the crystallization. The activation energies required for grain growth in amorphous $TiO_{2-x}N_x$ and TiO_2 samples were determined to be 1.6 and 1.7 kJ/mol, respectively. Those required for the phase transformation from amorphous to crystalline $TiO_{2-x}N_x$ and TiO_2 were determined to be 129 and 142 kJ/mol, respectively. A relatively low temperature was required for the phase transformation in NTP sample than in ATP sample. The fabricated N-doped TiO_2 photocatalyst absorbed the visible light showing two absorption edges; one in UV range due to titanium oxide as the main edge and the other due to nitrogen doping as a small shoulder. $TiO_{2-x}N_x$ photocatalyst demonstrated its photoactivity for photocurrent generation and decomposition of 2-propanol (IPA) under visible light irradiation ($\lambda \geqslant 420$ nm).

Keywords: TiO_2; $TiO_{2-x}N_x$; Visible light; Activation energy; Crystallization; Grain growth

1. Introduction

The era of photocatalysis-based energy conversion has been under evolution since 1972, when Fujishima and Honda [1] first reported the photocatalytic ability of TiO_2 to generate hydrogen by photosplitting of water. This inexpensive, high activity and high stability metal oxide semiconductor has also been in focus for its applications in organic and inorganic pollutant degradation to purify air and water and as a means to acquire superhydrophilicity of the solid surfaces [2–5]. However, TiO_2 is active only under ultraviolet (UV) light (wavelength <400 nm) due to its wide band gap of ca. 3.2 eV (for crystalline anatase phase at room temperature). As the fraction of UV radiation in solar spectrum is less than 5%, TiO_2 cannot be an intelligent candidate for an efficient exploitation of solar radiation (dominant visible light) on Earth. For smarter utilization of the dominant visible light part of the solar spectrum, and even for the indoor applications under weak interior lighting, photocatalyst absorbing visible light photons is a prerequisite. Consequently, search of visible light active photocatalysts is a subject of intense research today.

Recently, Sakatani and Koike [6] succeeded in fabricating nitrogen (N)-doped TiO_2 that absorbed visible light and showed activity for photocatalytic decomposition of acetaldehyde to CO_2 under visible light irradiation. Asahi et al. [7] reported that the electronic band structure of N-doped TiO_2, theoretically calculated by the full potential linearized augmented plane wave (FLAPW) method, predicted that it could be a good visible light active

*Corresponding author. Fax: +82 54 279 5528.
E-mail address: jlee@postech.ac.kr (J.S. Lee).

0022-4596/$ - see front matter © 2006 Elsevier Inc. All rights reserved.
doi:10.1016/j.jssc.2006.01.004

material. Irie et al. [8] reported nitrogen concentration dependence on photocatalytic activity of $TiO_{2-x}N_x$ powders. We have also succeeded [9] in preparing N-doped TiO_2 powders by a hydrothermal synthesis from $TiOSO_4$ and found their photocatalytic activity under visible light irradiation was higher than those prepared by hydrolytic synthesis from $TiCl_3$ [6].

Although $TiO_{2-x}N_x$ has been widely studied for the photocatalysis under visible light irradiation and the formation of anatase crystals is highly desired for high photocatalytic activities, the crystallization of the phase from amorphous precursor has not been investigated. In the present study, kinetics and crystallization behaviors of $TiO_{2-x}N_x$ formation in N-doped amorphous TiO_2 powders were investigated using X-ray diffraction (XRD) and differential scanning calorimetry (DSC). The activation energies for crystallization and grain growth of $TiO_{2-x}N_x$ were obtained from these data. The electronic and local coordination structures of N-doped TiO_2 crystal were investigated by X-ray absorption near edge structure (XANES) and X-ray photoelectron spectroscopy (XPS). Then, $TiO_{2-x}N_x$ photocatalyst was evaluated for photocurrent generation and decomposition of gaseous 2-propanol (IPA) under visible light irradiation ($\lambda \geqslant 420$ nm).

2. Experimental

2.1. Preparation and characterization of samples

Nitrogen-doped TiO_2 was prepared by the hydrolytic synthesis method (HSM) [6], in which aqueous ammonium hydroxide solution with an ammonia content of 28–30% (99.99%, Aldrich) was slowly added drop by drop to 20% titanium (III) chloride solution ($TiCl_3$, Kanto, contained 0.01% iron as the major impurity) for 30 min under N_2 flow in ice bath while continuously stirring and the suspension was stirred for 5 h to complete the reaction. After the completion of the reaction, the precipitates were filtered in air and washed several times with deionized water. Filtered powders were dried at 70 °C for 3–4 h in a convection oven. The samples obtained at this stage was called N-doped TiO_2 precursor (NTP), which was amorphous precipitated powers containing ammonia and titanium. Further this sample was calcined at 200–400 °C for 2 h in air flow in an electric furnace to obtain crystalline powders of $TiO_{2-x}N_x$.

For the purpose of comparison, amorphous TiO_2 precursor (ATP) sample was also prepared by sol–gel method (SGM) [10]. Thus 10 mL of titanium isoproxide $Ti(OCH(CH_3)_2)_4$ (97.0%, Aldrich) was dissolved in 50 mL of ethyl alcohol and then 3 mL of aqueous ammonium hydroxide solution were added. A homogeneous sol or colloidal solution was obtained after a few hours of vigorous stirring. White crystalline TiO_2 powders were formed by heating these ATP samples in air at various temperatures in the range of 200–400 °C for 2 h in an electric furnace.

These samples were characterized by powder XRD (Mac Science Co., M18XHF). The XRD peaks were compared with standard data in the Joint Committee Powder Diffraction Standards (JCPDS) for the identification of phases formed after thermal treatment. The optical properties were analyzed by UV-Visible diffuse reflectance spectrometer (Shimadzu, UV 2401). Morphologies of photocatalysts were investigated by transmission electron microscope (TEM) (JEOL JEM 2010F, Field Emission Electron Microscope). DSC (Shimadzu, DTA-50) was carried out in the temperature range of 30–900 °C with various heating rates of 10, 15, 20, 25 and 30 °C/min. IR spectra were recorded on a Jasco Valor-III spectrometer (KBr disk technique). X-ray absorption spectra (XAS) of the Ti *K*-edge were recorded on beamline BL3C1 of the Pohang Accelerator Laboratory (PAL) operating at 2.5 GeV with ca. 100–160 mA of the stored current. The radiation was monochromatized using a Si(111) double crystal monochromator to collect high-resolution XAS spectra. Data were collected at room temperature in a transmission mode. N_2 was used as a detector gas for both incident and transmitted beams. The absorption energy was calibrated by measuring XANES of Ti metal foil standard assigning the first inflection point in the absorbance–energy curve to 4970 eV. The XANES analysis was processed according to the following procedure using the program WinXAS 97 (Version 2.3); the spectra were normalized in absorbance by fitting the spectral region using a first-order polynomial function and subtracting this as background absorption. The chemical states of nitrogen in the precipitates and calcined samples were obtained from XPS measurements (VG Scientific, ESCALAB 220iXL) using Mg*K*α radiation (1253.6 eV). The binding energy calibration was performed using C1*s* peak in the background as the reference energy.

2.2. Photoelectrochemical and photocatalytic activities

Generation of photocurrent and photocatalytic degradation of IPA under visible light ($\lambda \geqslant 420$ nm) irradiation were studied as measures of photoelectrochemical and photocatalytic activities of the prepared samples. For photoelectrochemical measurements, [11] 50 mg of a photocatalyst was suspended in distilled water (75 mL) containing acetate (0.1 M) and Fe^{3+} (0.1 mM) as an electron donor and an acceptor, respectively, and the suspension pH was adjusted to 1.4 with $HClO_4$ to maintain the Fe^{3+} state. A platinum plate ($1.5 \times 1.5\,cm^2$, 0.125 mm thick, both sides exposed to the solution), a saturated calomel electrode (SCE), and a platinum gauze was immersed in the reactor as working (collector), reference, and counter electrodes, respectively. With continuous N_2 purging of the suspension, photocurrents were measured by applying a potential (+0.6 V vs. SCE) to the Pt working electrode using a potentiostat (EG&G).

Photocatalytic decomposition of gaseous IPA under visible light irradiation was performed in a closed gas

circulation system at room temperature using a high pressure Hg lamp (Oriel, 500 W). The UV-irradiation was removed by using a cutoff filter ($\lambda \geqslant 420$ nm). The photocatalytic reactor containing the glass plate was connected to the reaction system and sealed with silicone grease. The reactant gas of IPA was injected with a gas tight syringe into the gas circulation system with a total volume of 550 mL. The initial concentration of IPA was 1000 ppm balanced with air, which was controlled according to the gas chromatograph analyses. Upon reaching a steady state, visible light irradiation was initiated and continued for 3 h. The change of IPA concentration was followed by analysis with a gas chromatography (HP 5890 II) equipped with an FID detector (He carrier) and an AT-1 column.

3. Results and discussion

3.1. Characterization of prepared solids

It is interesting to observe that only the HSM with $TiCl_3$ produced N-doped TiO_2 after calcination, while SGM with titanium isoproxide produced pure TiO_2, although the same aqueous ammonium hydroxide was used as the hydrolyzing agent. The incorporation of nitrogen atom into TiO_2 lattice to form Ti–N bonds would require decomposition of ammonia, which may be favored under HSM conditions.

In order to compare the crystallization behavior of amorphous TiO_2 precursor sample (ATP) and N-doped TiO_2 precursor samples (NTP), their powder XRD patterns are shown in Figs. 1(A) and (B). Both precursor samples did not show any XRD peaks indicating that they were amorphous solids. Crystalline $TiO_{2-x}N_x$ and TiO_2 grew with increasing calcination temperatures. Crystallization behaviors of $TiO_{2-x}N_x$ and TiO_2 in NTP and ATP samples were very similar, both showing well-crystallized anatase phase upon heating to 400 °C. The direct formation of anatase TiO_2 crystallites is often observed at the nanoscale when TiO_2 nanocolloids are formed in a sol–gel synthesis [12]. In contrast, the present NTP and ATP samples crystallize to the anatase phase only on calcining. The formation of amorphous or crystalline forms of titania should depend on the details of preparation conditions. For example, the work by Gole et al. [12] used isopropyl alcohol as the solvent and acidic pH for preparation, while we used aqueous ammonia that gives a basic condition. Calcination at low temperatures (<400 °C) gives the anatase phase first that turns to the thermodynamically more stable rutile phase upon further heating above 500 °C.

The color of NTP sample was white, whereas that of crystalline $TiO_{2-x}N_x$ were yellow. Thus, the NTP is not yet nitrogen-doped TiO_2, i.e. TiO_2 lattice is not established yet as indicated by X-ray amorphous nature and the surface is covered by ammonium complex and its fragments. This powder shows the white color, and only when NTP sample is calcined, this material transforms to crystalline $TiO_{2-x}N_x$ of yellow color. Both ATP and crystalline TiO_2 were white. The morphologies of NTP sample and $TiO_{2-x}N_x$ were observed by TEM as shown in Fig. 2. The NTP sample showed an amorphous phase, which was consistent with the XRD pattern. But $TiO_{2-x}N_x$ showed nanoparticles with an irregular spherical shape and a particle size of ca. 20 nm. The UV-Vis diffuse reflectance spectra of these materials upon calcination at 400 °C are shown in Fig. 3. The TiO_2 anatase showed a single sharp edge, while $TiO_{2-x}N_x$ showed two absorption edges; the main edge due to the oxide at 390 nm and a weak shoulder due to nitrogen doping at 451 nm. This shoulder peak should be responsible for the visible light catalytic activity as discussed below.

In order to investigate the electronic and local coordination structures, the precipitate (NTP) and $TiO_{2-x}N_x$ were examined by XANES of Ti *K*-edge. The XANES represents electronic transition from an inner core level

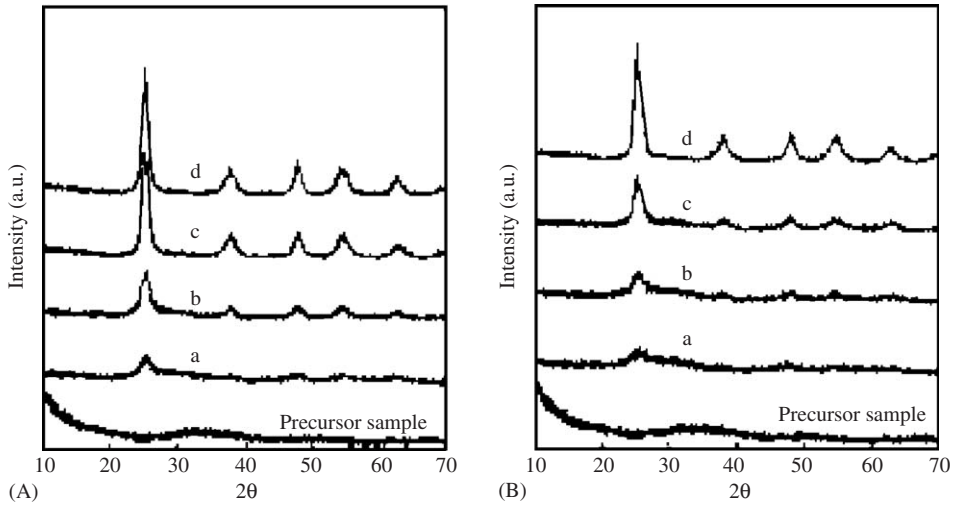

Fig. 1. XRD patterns of (A) a nitrogen-doped TiO_2 precursor samples, and of (B) a TiO_2 precursor samples heat-treated for 2 h at (a) 250 °C, (b) 300 °C, (c) 350 °C, and (d) 400 °C.

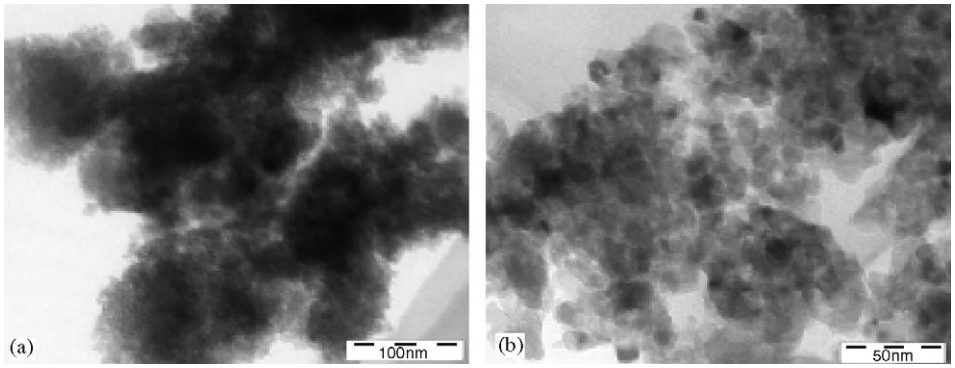

Fig. 2. TEM images of (a) NTP sample and (b) $TiO_{2-x}N_x$ obtained at 400 °C.

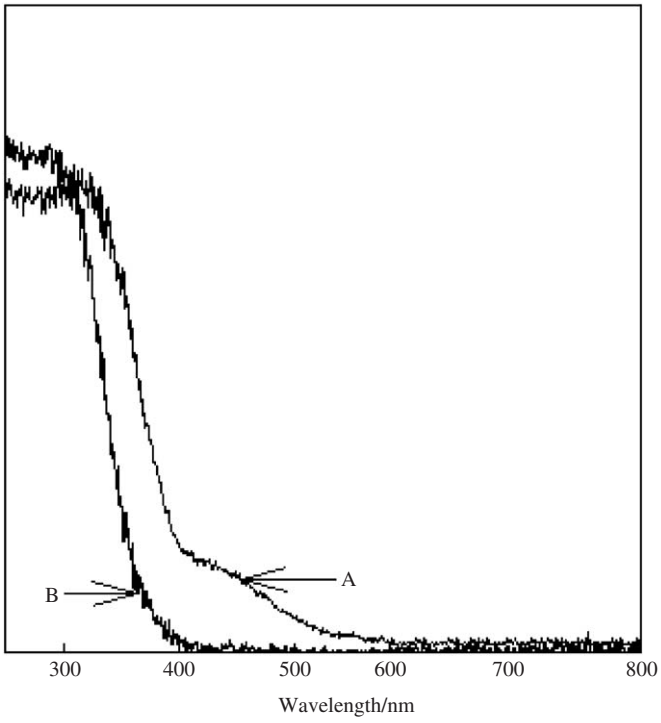

Fig. 3. UV-Vis diffuse reflectance of (A) $TiO_{2-x}N_x$ and (B) TiO_2 obtained at 400 °C.

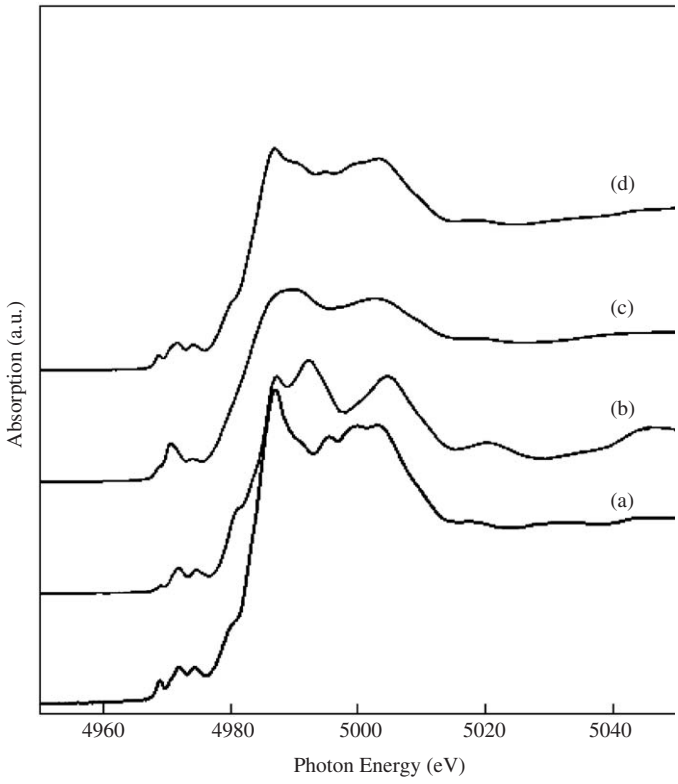

Fig. 4. Ti *K*-edge XANES spectra of (a) TiO_2 (anatase), (b) TiO_2 (rutile), (c) precipitate (NTP), and (d) $TiO_{2-x}N_x$ obtained at 400 °C.

to the outer unoccupied levels caused by X-ray absorption, thus giving information on the local electronic structure and coordination environment around an absorbing atom (Ti). Fig. 4 shows the Ti *K*-edge XANES spectra for the NTP sample (c) and crystalline $TiO_{2-x}N_x$ (d) obtained by calcination at 400 °C together with the reference samples of TiO_2 (anatase) (a), and TiO_2 (rutile) (b). The characteristic feature of the Ti *K*-edge spectra is the pre-edge peaks caused by the excitation of a 1*s* electron into an empty bound state derived from the d and p states of Ti and O. The weak triplet peaks indicated that Ti is located in an octahedral symmetry like in anatase and rutile structures. This feature is not clear for the amorphous NTP. The anatase and rutile structures could be differentiated by the fine structures of main absorption due to $1s \rightarrow 4p$ transition. The $TiO_{2-x}N_x$ sample showed the post-edge features very similar to those of anatase TiO_2 [13,14]. It indicates that even with the substitution of nitrogen into TiO_2 lattice, the sample preserves the initial local environment of the anatase structure.

Fig. 5 shows the FT-IR spectrum of (a) NTP sample-A (dried at 80 °C for 5 h), (b) NTP sample-B (dried at 80 °C for 1 day), and (b) crystalline $TiO_{2-x}N_x$ obtained by calcination of NTP at 400 °C. The wet precipitated powders contained large amounts of water, hydroxyl group, and ammonia. The presence of water was revealed by a strong bending vibration band at 1630 cm^{-1}, and a broad stretching vibration around 3400 cm^{-1}. The bands

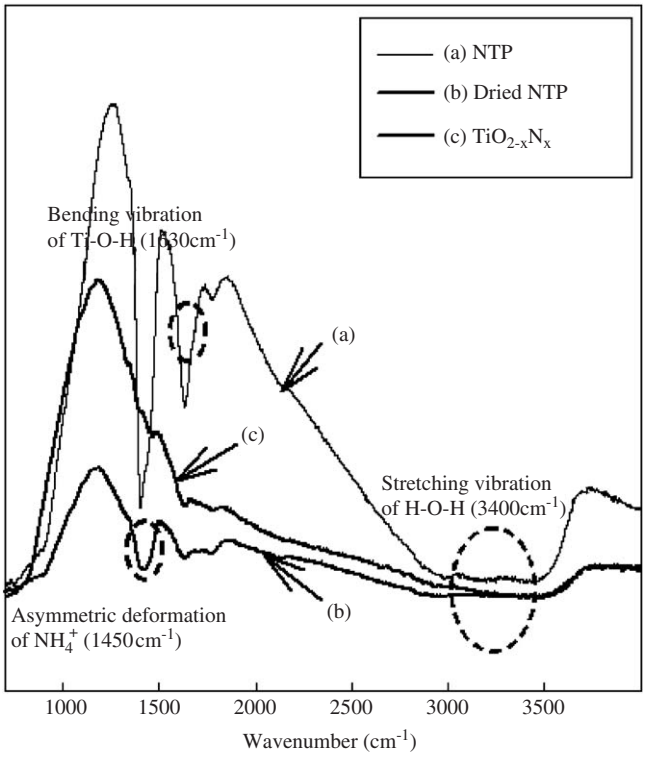

Fig. 5. FT-IR spectra of (a) NTP sample, (b) $TiO_{2-x}N_x$, and (c) TiO_2 (P25).

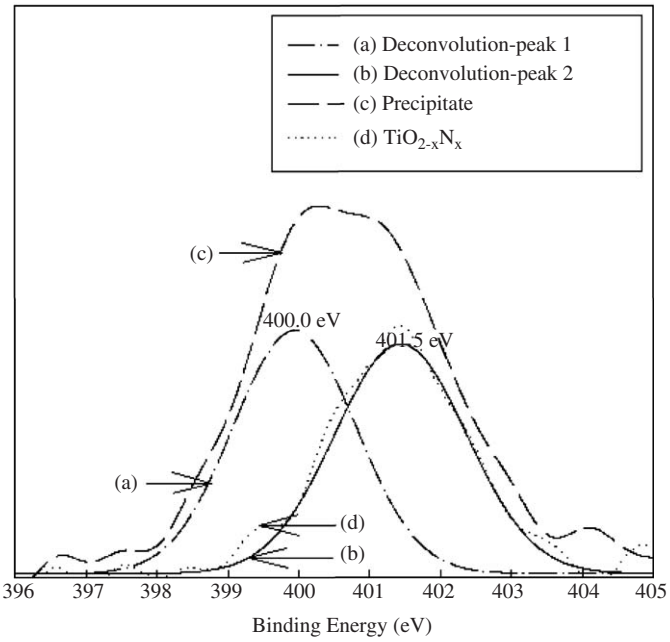

Fig. 6. XPS N $2p_{3/2}$ core-level spectra for (a) deconvolution-peak 1, (b) deconvolution-peak 2, (c) NTP sample, and (d) $TiO_{2-x}N_x$.

near 3400–3200 and 1600 cm^{-1} can be due to the stretching and asymmetric deformation vibrations of coordinated ammonia, respectively. These bands are nearly overlapped with those of water and hydroxyl group. A strong band near 1450 cm^{-1} and a shoulder near 1700 cm^{-1} (at the higher frequency side of NH_3 bending band) reveal the presence of ammonium cation (asymmetric deformation) in the NTP powder. After precipitate was dried at 80 °C for 1 day, most of bands were reduced in intensity or disappeared, indicating that merely adsorbed ammonia, water and hydroxyl group on surface of the precipitate were easily removed. But, the band near 1450 cm^{-1} assigned to the asymmetric deformation of NH_4^+ still remained although the intensity was greatly reduced.

The N 1*s* XPS spectrum of NTP sample showed a broad peak that could be deconvoluted into two peaks at 400.0 and 401.5 eV, as shown in Fig. 6. Upon calcination at 400 °C, obtained $TiO_{2-x}N_x$ showed a single peak that overlapped almost exactly with deconvoluted peak at 401.5 eV. This peak could be assigned to nitrogen interacting with Ti through Ti–N bond formation, while the peak at 400.0 eV could be assigned to the weakly adsorbed NH_4^+ observed in the FT-IR study (Fig. 5). There is a controversy over the assignment of N 1*s* XPS peak of $TiO_{2-x}N_x$ [12,15–18]. In the oxidation of TiN films, Saha and Tomkins [15] observed that N 1*s* XPS peak of TiN at 397 eV was transformed to three peaks at 396, 400, 402 eV. The peak at 396 eV was assigned to β-N (TiN), and two higher energy peaks to terminally bonded γ-N_2 of different degrees of screening. Martyanov et al. [16] attributed the high-energy peak to the surface bound NO species. However, they were also assigned to an atomic nitrogen species blue-shifted due to the presence of oxygen, i.e. N–Ti–O bond [12,17,18]. Since we did not observe surface NO species by FT-IR and the molecular nitrogen species is expected to be desorbed by calcination at 400 °C, we are of the opinion that the N 1*s* XPS peak at 401.5 eV may be due to the formation of the N–Ti–O bond. It should be noted that the precipitate containing ammonium cation and titanium is formed in the NTP state. Calcination decomposes NH_4^+ species and induces incorporation of nitrogen into TiO_2 lattice and removes NH_4^+ species from the surface. This is consistent with our previous result on hydrothermal synthesis of $(NH_4)_2Ti_3O_{7-x}N_x$ from $TiOSO_4$ in NH_4OH solution, followed by calcination to obtain $TiO_{2-x}N_x$ [9].

3.2. Kinetics of crystal growth

The average sizes of crystals (D_C) formed in NTP and ATP sample were estimated from the full-width at half-maxima (FWHM) of the (101) XRD peak of the anatase phase (the strongest peak in Figs. 1A and B) by using Scherrer's equation [19]; $D_C = \lambda/(\beta \cos\theta)$, where λ represents the wavelength of the X-ray radiation, θ the Braggle angle, and β the width of the XRD peak at half-maximum corrected for $K\alpha$ doublet separation and instrumental broadening. Crystallite sizes for the NTP and ATP samples are given in the inset of Fig. 7. Interestingly, it was found that at the same calcination temperature the crystallite size of TiO_2 formed in ATP sample was consistently smaller

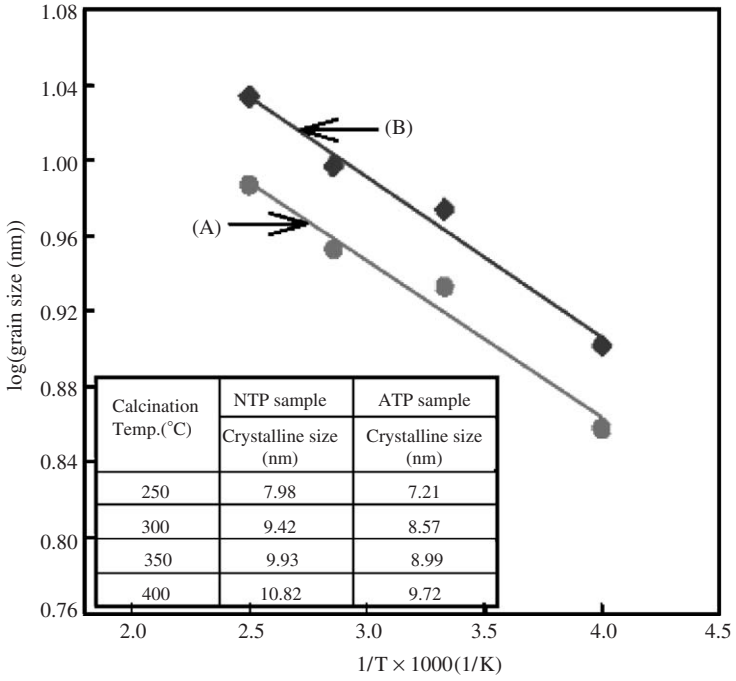

Calcination Temp.(°C)	NTP sample	ATP sample
	Crystalline size (nm)	Crystalline size (nm)
250	7.98	7.21
300	9.42	8.57
350	9.93	8.99
400	10.82	9.72

Fig. 7. A plot of log (grain size of $TiO_{2-x}N_x$ and TiO_2 in NTP (A) and ATP (B) samples heat-treated for 2 h at 250 °C, 300 °C, 350 °C, and 400 °C) versus the reciprocal of absolute temperature ($1/T$). The inset lists numerical data.

than that of $TiO_{2-x}N_x$ formed in NTP sample. $TiO_{2-x}N_x$ crystals in NTP sample grew faster relative to TiO_2 in ATP sample.

In order to quantify this behavior of crystal growth, the activation energy required for grain growth of $TiO_{2-x}N_x$ and TiO_2 in NTP sample and ATP sample was estimated by the Arrhenius plot of the crystallite sizes. According to Coble's theory [20], the activation energy of grain growth can be calculated by the Arrhenius equation

$$\mathrm{d}\ln k/\mathrm{d}T = E/RT^2, \tag{1}$$

where k is the specific reaction rate constant, E is the activation energy, T is the absolute temperature and R is the ideal gas constant. Jarcho et al. [21] discovered the value of k was related with the grain size directly. Thus, modification and integration of Eq. (1) becomes

$$\log D = (-E/2.303\,R)/T + A, \tag{2}$$

where D is the grain size and A is intercept. From a plot of $\log D$ versus the reciprocal of absolute temperature ($1/T$) from Eq. (2), one obtains a straight-line as shown in Fig. 7. The slope of the line gives the activation energies of grain growth of $TiO_{2-x}N_x$ and TiO_2 crystals in NTP and ATP samples. Activation energies of grain growth of $TiO_{2-x}N_x$ and TiO_2 were determined to be 1.6 and 1.7 kJ/mol, respectively. Thus, activation energy required for the formation of $TiO_{2-x}N_x$ crystals in NTP sample is almost the same as that for the formation of TiO_2 in ATP sample, although the crystallite size of $TiO_{2-x}N_x$ was consistently smaller than that of TiO_2 as described above.

Thermal behaviors of both NTP and ATP samples were investigated by DSC. The DSC curves of both samples in the temperature range of 50–900 °C with a heating rate of 10 °C/min are shown in Fig. 8. A single endothermic peak for each sample was identified in the DSC curves. These peaks in the DSC curves correspond to the transformation of the solid from amorphous to anatase phases and the results are in good accordance with XRD studies. The formation of anatase phase was indicated by a sharp endothermic peak at 360–399 °C for the NTP sample while that for the ATP sample was observed at 372–416 °C under the same DSC scan conditions. The inset in Fig. 9 shows the phase transition temperatures at different heating rates for both NTP and ATP samples as determined by DSC. The endothermic peaks are shifted to high temperatures with increasing the heating rates.

The activation energy for crystallization of $TiO_{2-x}N_x$ and TiO_2 in precursor samples could be calculated from the endothermic peak temperature values measured at different heating rates by using Kissinger's equations [22]

$$\ln(\Phi/T_p^2) = -E/RT_p + \text{const.}, \tag{3}$$

where Φ is the heating rate, T_p is the peak temperature and R is the ideal gas constant. As shown in Fig. 9, the plots of $\ln(\Phi/T_p^2)$ vs. $(1000/T_p)$ for the samples showed a straight line. The activation energy required for the phase transformation from NTP sample to $TiO_{2-x}N_x$ was calculated to be 129.3 kJ/mol from the slope of the straight line in Fig. 8(A). It was shown in the XPS study (Fig. 6) that the amorphous NTP sample contained two

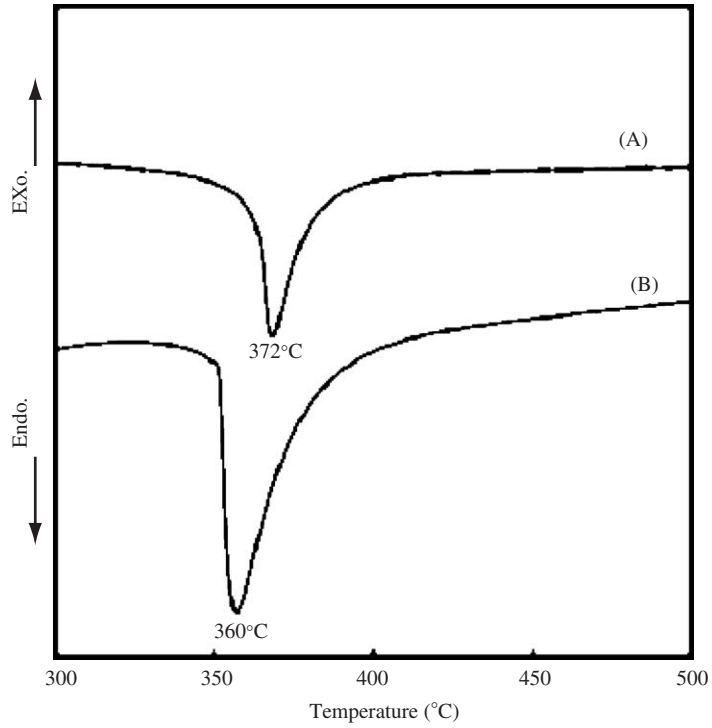

Fig. 8. Differential scanning calorimetry (DSC) curves of NTP (A) and ATP (B) samples.

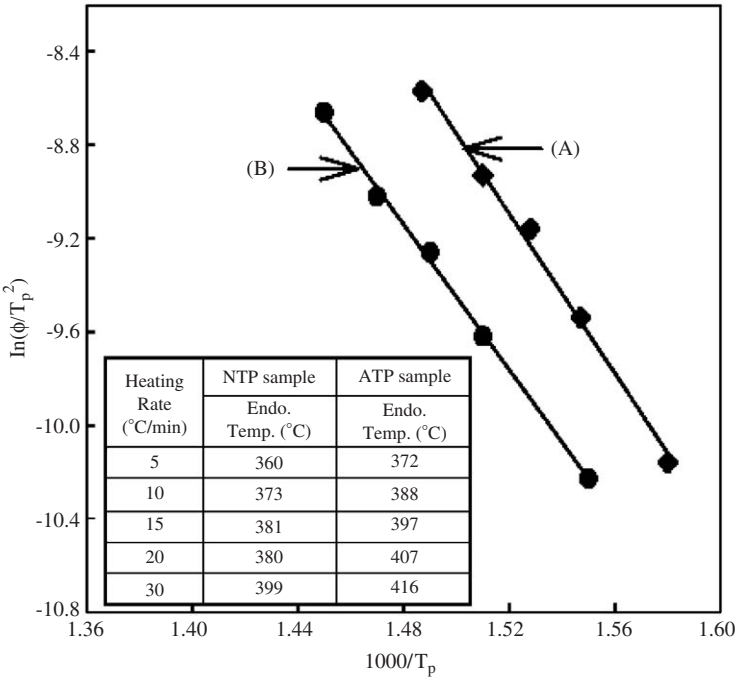

Heating Rate (°C/min)	NTP sample Endo. Temp. (°C)	ATP sample Endo. Temp. (°C)
5	360	372
10	373	388
15	381	397
20	380	407
30	399	416

Fig. 9. A plot to obtain the activation energies involved in the crystallization of amorphous phase in NTP (A) and ATP (B) samples. The inset lists numerical data.

nitrogen-containing species: one directly bonded to Ti and the other weakly adsorbed ammonia species [9]. Upon calcination to 400 °C, the latter adsorbed species left the surface leaving behind crystalline $TiO_{2-x}N_x$. Thus, the crystallization of $TiO_{2-x}N_x$ in NTP proceeds with the incorporation of nitrogen atoms into TiO_2 lattice. In case of the ATP sample, the energy required for the phase transformation from ATP sample to TiO_2 was calculated to be 142.1 kJ/mol from the slope of the straight line in Fig. 9(B). The lower activation energy required for phase

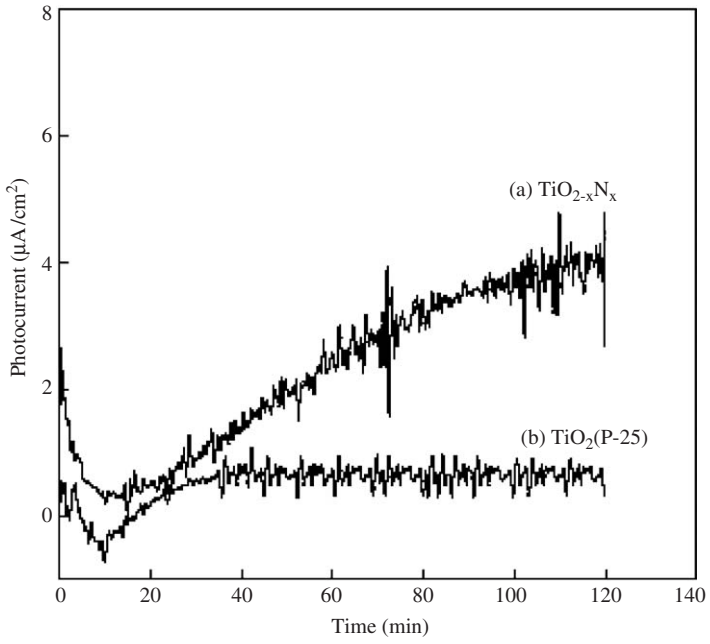

Fig. 10. Photocurrents generated from (a) $TiO_{2-x}N_x$, (b) TiO_2 (P25) under visible light ($\lambda \geqslant 420$ nm).

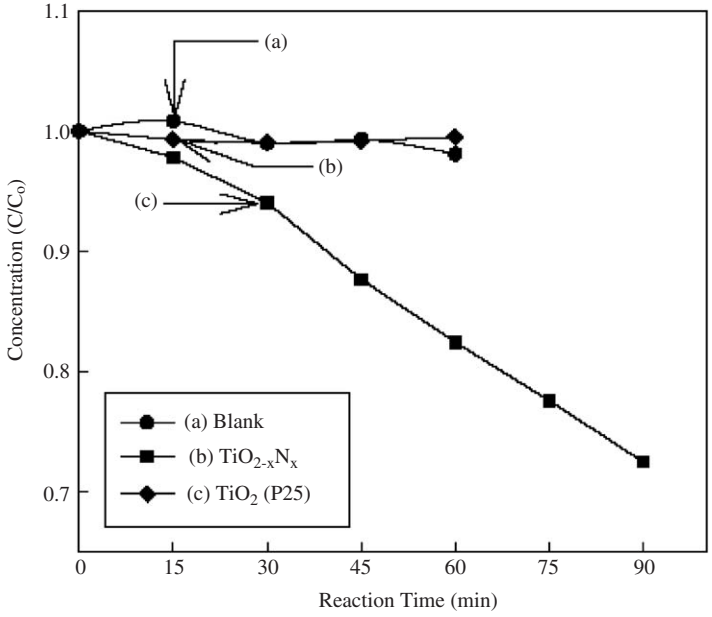

Fig. 11. Photocatalytic activity of IPA decomposition over (a) blank, (b) $TiO_{2-x}N_x$, and (c) TiO_2 (P25).

transformation in NTP samples can be attributed to the existence of nanodimensional nuclei contained in the amorphous powders, wherein the nitrogen species derived from ammonium cation probably facilitates the early phase transformation such as nitrogen impurity [16]. Since similar (amorphous) starting samples viz. ATP and NTP were used, the results clearly demonstrate the role of nitrogen species in precipitate that facilitates the rates of crystallization as well as crystal growth.

3.3. Photoelectrochemical and photocatalytic activity

As a measure of photoelectrochemical activity, we measured the generation of photocurrent under visible light irradiation ($\lambda \geqslant 420$ nm). As shown in Fig. 10, $TiO_{2-x}N_x$ generated photocurrent steadily, while TiO_2 (P25) as a reference sample did not generate photocurrent because this photocatalyst did not absorb visible light. This demonstrates that $TiO_{2-x}N_x$ could generate

photoelectrons and holes under visible light irradiation, and could become a visible light-responsive photocatalyst if the generated electrons/holes can reduce/oxidize organic and inorganic substrates.

To exploit its real photocatalytic activity under visible light irradiation, the oxidative decomposition of gaseous 2-propanol (IPA) was studied over $TiO_{2-x}N_x$. Fig. 11 shows the change of gaseous CO_2 concentration, generated as a result of the photodegradation of IPA over TiO_2 (P25), $TiO_{2-x}N_x$, as a function of irradiation time. The concentration of IPA decreased steadily under visible light ($\lambda \geqslant 420$ nm). During the decomposition of IPA, any intermediate product such as acetone was not observed. However, pure TiO_2 prepared from ATP or TiO_2 (P25) as a reference material had no photocatalytic activity for decomposition of IPA under the same condition. Thus, introduction of N into the TiO_2 lattice induces visible light absorption as indicated by the shoulder absorption peak in Fig. 3, which leads to visible light photocatalytic activity for IPA degradation. Pure TiO_2 is inactive under visible light irradiation because it absorbs only UV light.

4. Conclusion

Nitrogen-doped TiO_2 ($TiO_{2-x}N_x$) was prepared by a HSM using $TiCl_3$ and an ammonia solution followed by calcination at 400 °C. From FT-IR and XPS data, it was concluded that a complex containing ammonium ion and titanium was formed in the precipitate stage, while calcination drove weakly adsorbed ammonium species off the surface, decomposed the ammonia cation bound to the surface, and led to the incorporation of nitrogen atom into TiO_2 lattice. The activation energies required for the grain growth and phase formation of $TiO_{2-x}N_x$ in NTP sample were determined to be 1.6 kJ/mol and 129.3 kJ/mol, respectively. Relative to the TiO_2 crystallization in the precursor prepared by the SGM, phase-transformation kinetics of $TiO_{2-x}N_x$ was faster probably due to the presence of nitrogen species in the system. $TiO_{2-x}N_x$ demonstrated its photoactivity in photocurrent generation and degradation of 2-propanol under visible light ($\lambda \geqslant 420$ nm).

Acknowledgments

This work has been supported by the National Research Laboratory, BK-21 program, and Hydrogen Energy R&D Center.

References

[1] A. Fujishima, K. Honda, Nature 238 (1972) 37.
[2] T.H. Lim, S.D. Kim, Korean J. Chem. Eng. 21 (4) (2004) 905.
[3] M.R. Hoffman, S.T. Martin, W. Choi, D.W. Bahnemann, Chem. Rev. 95 (1995) 69.
[4] N. Serpone, E. Pelizzetti (Eds.), Photocatalysis Fundamental and Applications, Wiley, New York, 1989.
[5] Y. Na, S. Song, Y. Park, Korean J. Chem. Eng. 22 (2) (2005) 196.
[6] Y. Sakatani, H. Koike, Japan Patent, 2001, P2001-72419A.
[7] R. Asahi, T. Ohwaki, K. Aoki, Y. Taga, Science 293 (2001) 269.
[8] H. Irie, S. Watanabe, N. Yohino, K. Hashimoto, Chem. Commun. (2003) 1298.
[9] C.H. Rhee, S.W. Bae, J.S. Lee, Chem. Lett. 34 (5) (2005) 660.
[10] T. Nishide, F. Mizukami, Thin Solid Films 353 (1999) 67.
[11] H. Park, W. Choi, J. Photochem. Photobiol. A 159 (2003) 241.
[12] J.L. Gole, J.D. Stout, C. Burda, Y. Lou, X. Chen, J. Phys. Chem. B 108 (2004) 1230.
[13] L.A. Grunes, Phys. Rev. B 27 (1983) 2111.
[14] F. Babonneau, S. Doeuff, A. Leaustic, C. Sanchez, C. Cartier, M. Verdaguer, Inorg. Chem. 27 (1988) 3166.
[15] N.C. Saha, H.G. Tomkins, J. Appl. Phys. 72 (1992) 3072.
[16] I.N. Martyanov, S. Uma, S. Rodrigues, K.J. Klabunde, Chem. Commun. 21 (2004) 2476.
[17] E. Guyorgy, A. Perez del Pino, P. Serra, J.L. Morenza, Appl. Surf. Sci. 186 (2002) 130.
[18] H.Z. Wu, T.C. Cho, A. Misra, D.R. Anderson, J.K. Lambert, Thin Solid Films 191 (1990) 55.
[19] B.D. Cullity, Elements of X-ray Diffraction, second ed., Addison-Wesley Publishing Company, Inc., Reading, MA, 1978.
[20] R.L. Coble, J. Appl. Phys. 32 (1961) 787.
[21] M. Jarcho, C.H. Bolen, R.H. Doremus, J. Mater. Sci. 11 (1976) 2027.
[22] H.E. Kissinger, J. Res. Natl. Bur: Stand. (US) 57 (1956) 217.